CHEMISTRY OF MATERIALS
Article

Chem. Mater. **2010,** *22,* 6291–6296 6291
DOI:10.1021/cm101996u

One-Pot Aqueous Synthesis of Fe and Ag Core/Shell Nanoparticles

Kyler J. Carroll,[†] Daniel M. Hudgins,[†] Steven Spurgeon,[‡] Kennneth M. Kemner,[§] Bhoopesh Mishra,[§] Maxim I. Boyanov,[§] Lester W. Brown III,[†] Mitra L. Taheri,[‡] and Everett E. Carpenter*,[†]

[†]*Department of Chemistry, Virginia Commonwealth University, Richmond, Virginia 23284, United States,* [‡]*Department of Materials Science and Engineering, Drexel University, Philadelphia, Pennsylvania 19104, United States, and* [§]*Biosciences Division Argonne National Laboratory, Argonne, Illinois 60439, United States*

Received July 18, 2010. Revised Manuscript Received October 1, 2010

This article investigates a facile one-pot method for the synthesis of Fe and Ag core/shell nanoparticles by aqueous reduction under ambient conditions. We have shown that the injection time of silver nitrate into a reaction vessel containing aqueous ferrous salt, sodium borohydride, and sodium citrate is a vital parameter for the precise control of a desired core/shell structure. For example, if silver nitrate is injected one minute after sodium borohydride is added to the reaction vessel, Ag will nucleate first followed by Fe, creating monodisperse Ag/Fe core/shell nanoparticles. In contrast, if the introduction time is prolonged to 5 min, Fe nanoparticles will nucleate followed by Ag producing Fe/Ag nanoparticles. The composition, morphology, and magnetic behavior were investigated by X-ray absorption spectroscopy (XAS), X-ray photoelectron spectroscopy (XPS), X-ray diffraction (XRD), transmission electron microscopy (TEM), and room-temperature vibrating sample magnetometry (VSM). Fe/Ag core/shell nanoparticles with optical and magnetic functionality offer broad opportunities in medicine, catalysis, and chemical detection.

1. Introduction

Bimetallic nanoparticles with a core/shell morphology offer greater flexibility with enhanced properties as compared to their monometallic and bulk counterparts. The fabrication of bimetallic core/shell nanoparticles has thus attracted both fundamental and practical interest due to their potential applications in areas such as biosensing, catalysis, cancer therapy, and drug delivery.[1−4] Various types of core/shell structures have been fabricated where the core or shell consists of metals, semiconductors, and dielectric materials.[5−7] In addition, core/shell nanoparticles with both magnetic and optical properties offer a range of applications from magnetic separators to optical probes and recoverable catalysts.[8−11]

Several multistep synthetic methods have been reported to prepare bimetallic nanoparticles, including chemical reduction, microemulsion techniques, sonochemical reactions, γ-ray irradiation, and laser ablation.[1,12−20] These methods to create core/shell nanoparticles are typically done by using presynthesized Ag or Au particles which are then deposited onto presynthesized iron oxide nanoparticles by the use of functional groups such as amines and thiols.[21] Although these techniques have shown viability in synthesizing core/shell nanoparticles, the precise control of morphological properties is essential for many applications.

*To whom correspondence should be address. E-mail: ecarpenter2@vcu.edu. Tel: (804) 828-7508.

(1) Park, H.-Y.; Schadt, M. J.; Wang; Lim, I. I. S.; Njoki, P. N.; Kim, S. H.; Jang, M.-Y.; Luo, J.; Zhong, C.-J. *Langmuir* **2007**, *23*, 9050.
(2) Lee, I. S.; Lee, N.; Park, J.; Kim, B. H.; Yi, Y.-W.; Kim, T.; Kim, T. K.; Lee, I. H.; Paik, S. R.; Hyeon, T. *J. Am. Chem. Soc.* **2006**, *128*, 10658.
(3) Lu, P.; Teranishi, T.; Asakura, K.; Miyake, M.; Toshima, N. *J. Phys. Chem. B* **1999**, *103*, 9673.
(4) Gupta, A. K.; Gupta, M. *Biomaterials* **2005**, *26*, 3995.
(5) Sobal, N. S.; Ebels, U.; Möhwald, H.; Giersig, M. *J. Phys. Chem. B* **2003**, *107*, 7351.
(6) Gerion, D.; Pinaud, F.; Williams, S. C.; Parak, W. J.; Zanchet, D.; Weiss, S.; Alivisatos, A. P. *J. Phys. Chem. B* **2001**, *105*, 8861.
(7) Sao-Joao, S.; Giorgio, S.; Penisson, J. M.; Chapon, C.; Bourgeois, S.; Henry, C. *J. Phys. Chem. B* **2004**, *109*, 342.
(8) Jun, B.-H.; Noh, M. S.; Kim, J.; Kim, G.; Kang, H.; Kim, M.-S.; Seo, Y.-T.; Baek, J.; Kim, J.-H.; Park, J.; Kim, S.; Kim, Y.-K.; Hyeon, T.; Cho, M.-H.; Jeong, D. H.; Lee, Y.-S. Small **2009**, *9999*, NA.
(9) Kim, K.; Jing Jan, H.; Shin Soo, K. *Analyst* **2009**, *134*, 208.
(10) Noh, M. S.; Jun, B.-H.; Kim, S.; Kang, H.; Woo, M.-A.; Minai-Tehrani, A.; Kim, J.-E.; Kim, J.; Park, J.; Lim, H.-T.; Park, S.-C.; Hyeon, T.; Kim, Y.-K.; Jeong, D. H.; Lee, Y.-S.; Cho, M.-H. *Biomaterials* **2009**, *30*, 3915.
(11) Radwan, F. N.; Carroll, K. J.; Carpenter, E. E. *J. Appl. Phys.* **2010**, *107*, 09B515.
(12) Lu, L.; Zhang, W.; Wang, D.; Xu, X.; Miao, J.; Jiang, Y. *Mater. Lett.* **2010**, *64*, 1732.
(13) Bala, T.; Bhame, S. D.; Joy, P. A.; Prasad, B. L. V.; Sastry, M. *J. Mater. Chem.* **2004**, *14*, 2941.
(14) Lin, J.; Zhou, W.; Kumbhar, A.; Wiemann, J.; Fang, J.; Carpenter, E. E.; O'Connor, C. J. *J. Solid State Chem.* **2001**, *159*, 26.
(15) Kim, K.; Jang, H. J.; Shin, K. S. *Analyst* **2009**, *134*, 308.
(16) Kinoshita, T.; Seino, S.; Mizukoshi, Y.; Otome, Y.; Nakagawa, T.; Okitsu, K.; Yamamoto, T. A. *J. Magn. Magn. Mater.* **2005**, *293*, 106.
(17) Zhang, J.; Post, M.; Veres, T.; Jakubek, Z. J.; Guan, J.; Wang, D.; Normandin, F.; Deslandes, Y.; Simard, B. *J. Phys. Chem. B* **2006**, *110*, 7122.
(18) Mandal, M.; Kundu, S.; Ghosh, S. K.; Panigrahi, S.; Sau, T. K.; Yusuf, S. M.; Pal, T. *J. Colloid Interface Sci.* **2005**, *286*, 187.
(19) Stoeva, S. I.; Huo, F.; Lee, J.-S.; Mirkin, C. A. *J. Am. Chem. Soc.* **2005**, *127*, 15362.
(20) Wang, L.; Luo, J.; Fan, Q.; Suzuki, M.; Suzuki, I. S.; Engelhard, M. H.; Lin, Y.; Kim, N.; Wang, J. Q.; Zhong, C.-J. *J. Phys. Chem. B* **2005**, *109*, 21593.
(21) Levin, C. S.; Hofmann, C.; Ali, T. A.; Kelly, A. T.; Morosan, E.; Nordlander, P.; Whitmire, K. H.; Halas, N. J. *ACS Nano* **2009**, *3*, 1379.

Published on Web 11/08/2010

In this study, we utilize a simplistic one-pot aqueous synthesis of Fe and Ag core/shell nanoparticles using sodium borohydride and sodium citrate under ambient conditions. Although Fe/Au nanoparticles have been the subject of intense research,[22−30] recently there has been increasing interest in the design of Fe/Ag core/shell nanoparticles due to a much larger extinction coefficient of the surface plasmon band relative to Au.[8−10,31] In addition, Ag nanoparticles exhibit a plasmon band between 390 and 420 nm, whereas Au nanoparticles exhibit a plasmon band between 520 and 580 nm.[32] Therefore, Ag nanoparticles have the ability to offer new application opportunities that can rely on the differences in the position and intensity of the surface plasmon band, relative to Au.

Recently, Lu et al. reported a two-step process to create monodisperse Fe/Ag core−shell nanoparticles to achieve higher saturation magnetization relative to the conventional iron oxide cores.[12] However, we report on the formation of Fe/Ag core/shell nanoparticles by a one-pot method. We have shown that by changing the time in which the $AgNO_3$ solution is added to the reduction of Fe nanoparticles, we are able to create either Ag/Fe or Fe/Ag core−shell nanoparticles. For example, if silver nitrate is injected 1 min after sodium borohydride is added to the reaction vessel, Ag will nucleate first followed by Fe, creating monodisperse Ag/Fe core/shell structures. In contrast, if the introduction time is prolonged to 5 min, Fe nanoparticles will nucleate followed by Ag growth producing Fe/Ag nanoparticles. This work offers not only a facile one-pot method for creating various types of core/shell structures by controlling one parameter, but it also has the ability to be easily scalable for industrial synthesis due to the inexpensive materials, short reaction times, and ambient conditions. Because of their potentially useful optical activity and magnetic properties, we have focused on the Ag−Fe system, although we believe the general approach described below may be applicable to other important materials systems as well.

2. Experimental Section

Iron(II) sulfate heptahydrate ($FeSO_4 \cdot 7H_2O$), silver nitrate ($AgNO_3$), and sodium borohydride ($NaBH_4$) were purchased from ACROS Organics. Trisodium citrate dihydrate was purchased from Mallinckrodt chemicals. All chemicals were used as received and without further purification.

Stock 0.5 M $AgNO_3$ aqueous solutions were made and kept under dark conditions in an amber bottle to maintain uniformity between experiments. $AgNO_3$ stock solutions were discarded after 1 week to ensure minimal photodegredation. In each case, the synthesis was carried out under ambient conditions.

Preparation of Fe nanoparticles. Fe nanoparticles were synthesized as previously reported.[33,34] Briefly, to produce consistent spherical Fe nanoparticles, a borohydride to Fe ratio, and an Fe to citrate ratio were kept at 2:1 and 10:1, respectively. First, a 2.0 L solution containing 4.6 mM $FeSO_4$ and 0.46 mM trisodium citrate dihydrate was mixed using magnetic stirring. $NaBH_4$ (8.8 mM) was added to the mixture and allowed to react for 10 min. The solution was quenched with ethanol several times and magnetically separated using a rare earth magnet. After washing was complete, the remaining ethanol was decanted and the particles were placed in a vacuum oven at room temperature to dry.

Preparation of Fe/Ag and Ag/Fe Core/Shell Nanoparticles. By varying the injection time of $AgNO_3$ to the reaction vessel containing sodium citrate, $FeSO_4$, water, and $NaBH_4$, we were able to manipulate which metal resided in the core and the shell.

Several ratios of Ag/Fe were analyzed as well as times between the addition of $NaBH_4$ and $AgNO_3$. The Ag precursor addition time is an important parameter for creating the desired core/shell structures and will be discussed in detail below. In the reaction, sodium citrate and iron sulfate are added to 2.0 L of DI-H_2O followed by the addition of $NaBH_4$. The solution turns from clear to a gray/black color after the addition of $NaBH_4$.

Characterization. The dried powders were characterized by X-ray diffraction (XRD), transmission electron microscopy (TEM), X-ray photoelectron spectroscopy (XPS), X-ray absorption spectroscopy (XAS), and vibrating sample magnetometry (VSM) for the determination of phase, morphology, and magnetic properties. XRD measurements were performed using a PANalytical X'pert pro diffractometer at a scanning step of 0.05° with a 2θ range from 20 to 120° using a graphite monochromated Cu−K_α radiation source. Samples were ground and pressed onto a no background, low volume holder. Room-temperature magnetometry was performed on a Lakeshore Cryotonics Inc. model 7300 VSM with an applied field between −10 000 and 10 000 Oe. The powders were characterized using a JEOL JEM2100 transmission electron microscope and imaged in bright field at an accelerating voltage of 200 keV. Samples were mounted on a 300 mesh lacey carbon TEM grid. The particles were first ultrasonicated in solution for about 9 min. During this time, lacey carbon grids were immersed in chloroform for 30 s to dissolve their Formvar-backing layer. After sonication, a pipet was used to transfer a drop of each nanoparticle solution onto a grid. The grids were then placed on a hot plate at 50 °C and allowed to dry for an hour. After drying, each sample was mounted in the instrument. UV−vis absorption analysis was carried out using a Hewlett-Packard 8453 photodiode spectrophotometer. Solutions were prepared in an aqueous environment using a quartz cuvette with a 1 cm path length. X-ray photoelectron spectroscopy (XPS) was performed on a Thermo Scientific ESCALAB 250 microprobe with a focused monochromatic Al Kα X-ray (1486.6 eV) source and a 180°

(22) Cho, S. J.; Idrobo, J. C.; Olamit, J.; Liu, K.; Browning, N. D.; Kauzlarich, S. M. *Chem. Mater.* **2005**, *17*, 3181.
(23) Cho, S. J.; Jarrett, B. R.; Louie, A. Y.; Kauzlarich, S. M. *Nanotechnology* **2006**, *17*, 640.
(24) Cho, S. J.; Kauzlarich, S. M.; Olamit, J.; Liu, K.; Grandjean, F.; Rebbouh, L.; Long, G. J. *J. Appl. Phys.* **2004**, *95*, 6804.
(25) Cho, S. J.; Shahin, A. M.; Long, G. J.; Davies, J. E.; Liu, K.; Grandjean, F.; Kauzlarich, S. M. *Chem. Mater.* **2006**, *18*, 960.
(26) Lin, J.; Zhou, W. L.; Kumbhar, A.; Wiemann, J.; Fang, J. Y.; Carpenter, E. E.; O'Connor, C. J. *J. Solid State Chem.* **2001**, *159*, 26.
(27) Srikanth, H.; Carpenter, E. E.; Spinu, L.; Wiggins, J.; Zhou, W. L.; O'Connor, C. J. *Mater. Sci. Eng., A* **2001**, *304*, 901.
(28) Wiggins, J.; Carpenter, E. E.; O'Connor, C. J. *J. Appl. Phys.* **2000**, *87*, 5651.
(29) Zhou, W. L.; Carpenter, E. E.; Lin, J.; Kumbhar, A.; Sims, J.; O'Connor, C. J. *Eur. Phys. J. D* **2001**, *16*, 289.
(30) Gole, A.; Stone, J. W.; Gemmill, W. R.; zur Loye, H.-C.; Murphy, C. J. *Langmuir* **2008**, *24*, 6232.
(31) Lee, K. J.; Nallathamby, P. D.; Browning, L. M.; Osgood, C. J.; Xu, X.-H. N. *ACS Nano* **2007**, *1*, 133.
(32) Cao, Jin, R.; Mirkin, C. A. *J. Am. Chem. Soc.* **2001**, *123*, 7961.
(33) Carroll, K. J.; Hudgins, D. M.; Brown, L. W., Iii; Yoon, S. D.; Heiman, D.; Harris, V. G.; Carpenter, E. E. *J. Appl. Phys.* **2010**, *107*, 09A303.
(34) Carroll, K. J.; Pitts, J. A.; Zhang, K.; Pradhan, A. K.; Carpenter, E. E. *J. Appl. Phys.* **2010**, *107*, 09A302.

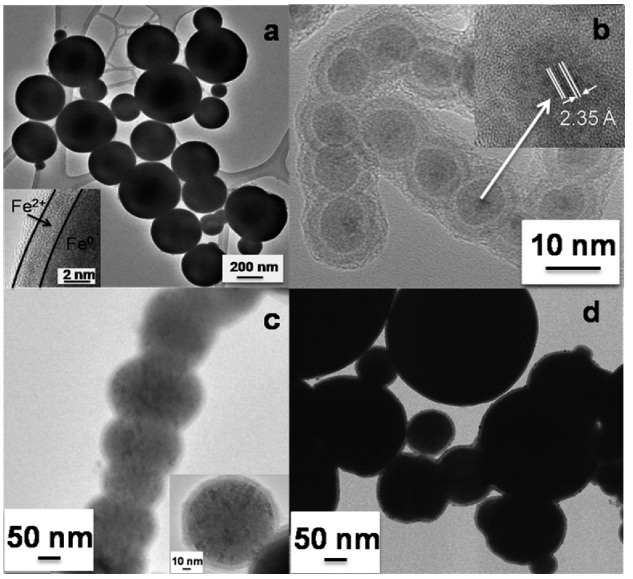

Figure 1. High-resolution TEM images of (a) as-synthesized Fe nanoparticles, (b) Ag/Fe nanoparticles showing a clear distinction between the core (Ag) and shell (FeB/Fe_2B), (c) Fe/Ag nanoparticles, and (d) Fe nanoparticles with islanding of Ag.

hemispherical analyzer with a 6-element multichannel detector. The incident X-ray beam was 45° off normal to the sample while the X-ray photoelectron detector was normal to the sample. Charge compensation was employed during data collection using an internal flood gun (2 eV electrons) and a low-energy Ar^+ external flood gun. Binding energies of the photoelectron are corrected to the aliphatic hydrocarbon C 1s peak at 284.6 eV. A Large area XL magnetic lens with a 500 μm spot size in constant analyzer energy (CAE) mode was utilized with a pass energy of 20 eV. Thirty scans per region were taken with a step size of 0.100 eV. The powdered samples were pressed onto a strip of indium foil and mounted on a sample holder using double-sided carbon tape. Fe K edge (7112 eV) XAFS measurements (encompassing both XANES and EXAFS) were performed at the MRCAT beamline 10-BM at the Advanced Photon Source (APS). Samples were measured in transmission mode. The data quality is represented in the k-weighted spectra (see S1 in the Supporting Information). The energy of the incident X-rays was scanned using a Si(111) reflection plane of a cryogenically cooled double-crystal monochromator. Detailed XAFS analysis can be found in the Supporting Information.

3. Results and Discussion

Figure 1A−D depicts high-resolution transmission electron microscopy images. TEM observations indicates that if the reaction is left to react for 15 min, the resulting particles are approximately 5 nm Fe nanoparticles encased in 200 nm bundles(Figure 1a), as reported by others.[34] Typically, in an aqueous reaction where sodium borohydride is used as the reducing agent, the resulting Fe nanoparticles are in the form of borides (FeB/Fe_2B).[35−37] However, Ekirt et al. have recently found that by adding a capping agent, such as sodium citrate, the resulting Fe nanoparticles are in the form of 5 nm body-centered cubic (bcc) Fe with a protective citrate layer encapsulating the particles and preventing oxidation.[38] This has been observed and confirmed in our work by both XRD and VSM data, which show diffraction lines of bcc-Fe and magnetization saturation values of ~175 emu/g (see Figures S4 and S5 in the Supporting Information).

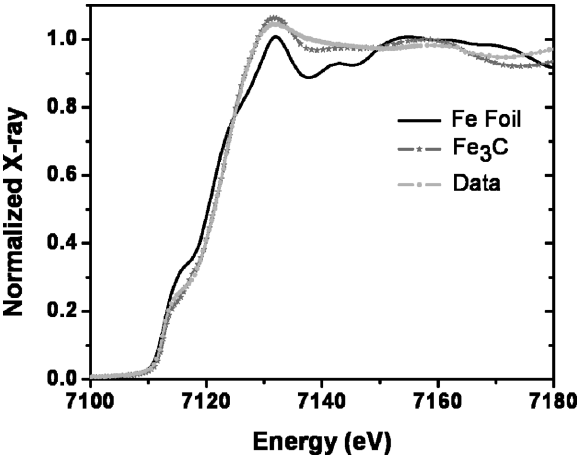

Figure 2. XANES spectra of the Fe/Ag core/shell nanoparticles plotted with spectra collected from Fe metal foil and Fe_3C standards.

Alternatively, an injection of aqueous $AgNO_3$ 1 min past the addition of $NaBH_4$ into the reaction vessel results in the formation of monodisperse Ag core and Fe shell nanoparticles with a total diameter of 12 nm (4 nm Ag core and an 8 nm Fe shell) (Figure 1b). The *d*-spacing of the core was found to be 2.350 Å, which was measured from the HR-TEM image. This spacing is consistent with that of the (111) reflection of face-centered cubic (fcc) Ag.[39] Figure 1c represents an injection of aqueous $AgNO_3$ 5 min past the addition of $NaBH_4$ into the reaction vessel and shows the formation of Fe/Ag core/shell nanoparticles. Lastly, if the injection of aqueous $AgNO_3$ is prolonged to 15 min, the formation of 200 nm Fe clusters (as in 1a) with a discontinuous shell (islanding) of Ag is shown (Figure 1d).

To gain a better understanding of the structural nature of the formed core/shell nanoparticles XAFS measurements were conducted. Figure 2 shows the Fe K-edge XANES data of the as-synthesized Ag/Fe core/shell nanoparticles plotted with spectra collected from Fe_3C and from Fe metal foil. The pre-edge and edge features of the Fe nanoparticles are clearly different from bcc Fe and match well with the Fe_3C standard. Postedge features are susceptible to longer-range structure and appear different from both the Fe_3C standard and Fe foil. Given the 8 nm thickness of the Fe shell of the core/shell nanoparticles as shown by TEM, the postedge features could not be unambiguously assigned from XANES. EXAFS analysis rules out a bcc Fe coordination environment. However, inclusion of carbon or boron atoms in addition to Fe atoms in the first shell resulted in statistically significant improvement in the fitting results of the sample.

(35) Glavee, G. N.; Klabunde, K. J.; Sorensen, C. M.; Hadjipanayis, G. C. *Langmuir* **1994**, *10*, 4726.
(36) Glavee, G. N.; Klabunde, K. J.; Sorensen, C. M.; Hadjipanayis, G. C. *Langmuir* **1993**, *9*, 162.
(37) Glavee, G. N.; Klabunde, K. J.; Sorensen, C. M.; Hadjapanayis, G. C. *Langmuir* **1992**, *8*, 771.
(38) Ekeirt, T. F., University of Delaware, 2010.
(39) Mishra, Y. K.; Mohapatra, S.; Kabiraj, D.; Mohanta, B.; Lalla, N. P.; Pivin, J. C.; Avasthi, D. K. *Scr. Mater.* **2007**, *56*, 629.

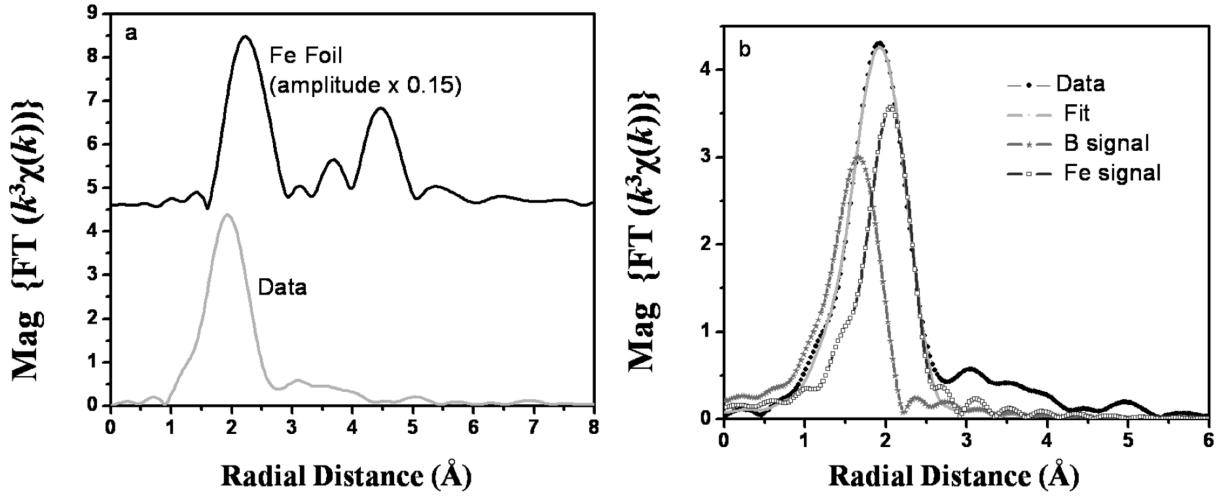

Figure 3. (a) Comparison of Fourier Transform EXAFS spectra of Fe foil and Ag/Fe; (b) Fourier Transform magnitude of the data and the fit plotted with the contributions of Fe and B signals.

Table 1. Fitting with Fe and B Paths

path	N	R (Å)	σ^2 ($\times 10^{-3}$ Å^{-2})	χ^2_v	R factor	E_o (eV)
Fe−B	2.82 ± 0.14	2.18 ± 0.01	15.5[a]	67	0.0014	-5.9 ± 1.8
Fe−Fe	3.52 ± 0.21	2.63 ± 0.01	11.8[a]			

[a] Fixed to best fit value.

Hence, the two most reasonable models (i.e., carbide and boride) will be discussed further.

Comparisons of the FT EXAFS data (Figure 3a) of the Fe nanoparticles to that of bcc Fe metal show that the first FT peak is of much smaller amplitude and shifted to shorter distances, similar to what is observed by Qadri et al. with Fe-boride nanoparticles.[40] Since $FeSO_4$ was reduced with borohydride as the starting material, formation of Fe-boride is consistent with the chemical composition of the system. An Fe-boride standard spectrum was not available for comparison. The Ag/Fe spectrum also showed similarity to the Fe-carbide standard. However, Fe-carbide can be excluded on the basis of the chemical composition of the material. Below we discuss a fitting model based on the observed spectral similarity between the unknown sample and Fe-boride.

A single Fe shell does not reproduce well with the main FT peak in a fitting procedure. The inclusion of B atoms in addition to Fe atoms in the first shell resulted in statistically significant improvement in the fitting results of the sample. Fitting parameters for Fe-boride are given in Table 1. Magnitudes of the Fourier transform data and fit with the contribution of Fe and B signals are shown in Figure 3b. Fitting with Fe and B signals result in an average coordination numbers of ~3.5 Fe atoms and ~2.8 B atoms around Fe at an average distance of 2.63 and 2.18 Å, respectively. These distances match well both with the previously reported crystallography as well as EXAFS analysis of Fe-boride compounds.[40,41] However, the coordination number reported in our study is smaller than the typical Fe and B coordination number in FeB/Fe_2B nanoparticles. This can possibly arise from a thin coating of FeB/Fe_2B over a Ag core, consistent with the TEM results. The lack of second and higher shell structure in the Fourier transform of the sample (Figure 3a) is also consistent with a thin disordered Fe-boride coating over a Ag core. Since the Fe−Fe distance reported in this study (2.63 Å) falls in the distance range seen for both FeB (2.62−2.95 Å) and Fe_2B (2.40−2.72 Å), the EXAFS analysis cannot unequivocally distinguish between the formation of FeB from Fe_2B coating over the Ag core.[41]

Figure 4a presents the XPS survey scan of freshly prepared Fe/Ag core/shell nanoparticles. The photoelectron peaks reveal that the nanoparticle surface consists of mainly Ag, O, C and Fe, as well as trace amounts of B. C1s and O1s regions scans suggest that the nanoparticle surface contains some adsorbed citrate, which is consistent with literature.[38] Two peaks at ~192 and ~188 eV in the B1s region spectra could be due to a oxidized boron (borate) adsorbed on the surface or B from FeB/Fe_2B, respectively. Both of which are common with borohydride reduction.[42] Detailed XPS region scans for Fe2p are shown in the Supporting Information (Figures S2 and S3). Shakeup and satellite peaks can be seen at 712 and 716 eV.[43,44] Literature suggests that the smaller peak at 706.82 eV, which typically corresponds to elemental Fe

(40) Qadri, S. B.; Dinderman, M. A.; Dressick, W. J.; Schoen, P. E.; Lubitz, P.; He, J. H.; Tonucci, R. J.; Cross, J. *Appl. Phys. A: Mater. Sci. Process* **2007**, *89*, 493.
(41) Kapfenberger, C.; Albert, B.; Pottgen, R.; Huppertz, H. *Z. Kristallogr.* **2006**, *221*, 477.
(42) Nurmi, J. T.; Tratnyek, P. G.; Sarathy, V.; Baer, D. R.; Amonette, J. E.; Pecher, K.; Wang, C. M.; Linehan, J. C.; Matson, D. W.; Penn, R. L.; Driessen, M. D. *Environ. Sci. Technol.* **2005**, *39*, 1221.
(43) Joyner, D. J.; Johnson, O.; Hercules, D. M. *J. Am. Chem. Soc.* **1980**, *102*, 1910.
(44) Grosvenor, A. P.; Kobe, B. A.; Biesinger, M. C.; McIntyre, N. S. *Surf. Interface Anal.* **2004**, *36*, 1564.

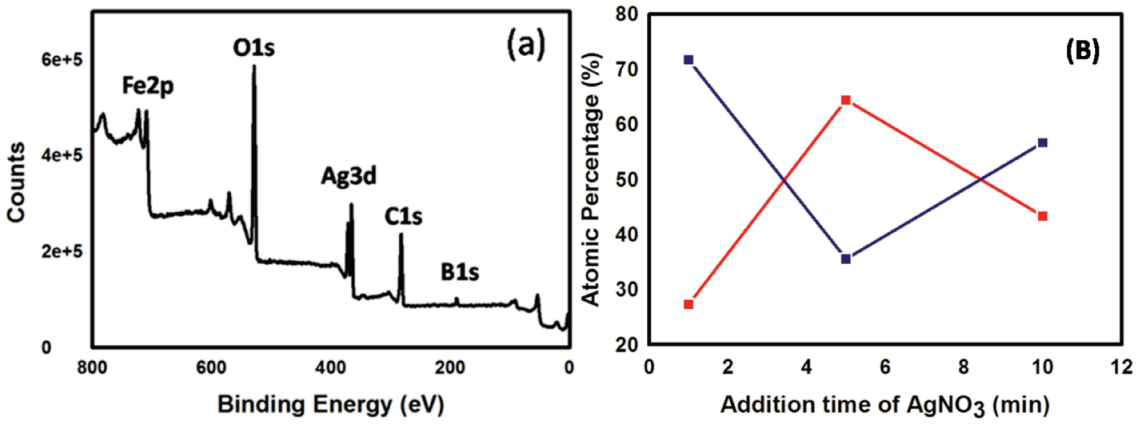

Figure 4. (a) XPS survey scan of a representative Fe/Ag core/shell nanoparticle. (b) Atomic percentage of Fe2p (blue) and Ag3d (red) as a function of $AgNO_3$ addition time determined by survey scans and standard sensitivity factors. The plotted solid lines are intended as a guide to the eye.

Table 2. XPS Binding Energies of FeB, Fe_2B, and Elemental Fe Core Levels

	literature			observed			
	Fe2p				Fe2p		
	1/2	3/2	B1s		1/2	3/2	B1s
Fe	720	706.9−707.4		1 min	719.5	706.9	187.77
FeB	720.3	707.2	188.1	5 min	719.98	707	187.84
Fe_2B	720.2	707.1	188.1	10 min	719.77	706.98	187.92

could also be also associated with FeB/Fe_2B.[45−50] Table 2 lists the binding energies of the Fe and B core levels observed at various $AgNO_3$ introduction times and is compared to the literature core level values. Binding energy shifts for the corresponding elemental Fe and boride core levels are very small (within 0.3 eV) and the B1s level binding energies are very similar, making the identification of elemental Fe and FeB/Fe_2B very difficult, especially because the literature values for elemental Fe shift from 706.9 to 707.4 eV. Photoelectron peaks at ~710 and ~721 eV correspond to the binding energies of Fe $2p_{3/2}$ and $2p_{1/2}$ for Fe^{2+}, respectively. Figure S5 in the Supporting Information describes how the amount of Fe^{2+} decreases depending on the introduction time of $AgNO_3$. For example, the particles that were formed after one minute $AgNO_3$ introduction formed Ag/Fe core/shell structures. Using the information from the TEM data, which suggests an 8 nm shell, it can be hypothesized that the reactivity of the Fe is increased, resulting in the surface of the nanoparticle to become easily oxidized, thus having a larger intensity of Fe^{2+}. However, the particles that were formed after 5 min of $AgNO_3$ introduction formed Fe/Ag core/shell structures, whereas in this case, the Ag would prevent the surface of the Fe from being oxidized.

(45) Johnson, O.; Joyner, D. J.; Hercules, D. M. *J. Phys. Chem.* **1980**, *84*, 542.
(46) Joyner, D. J.; Hercules, D. M. *J. Chem. Phys.* **1980**, *72*, 1095.
(47) Joyner, D. J.; Johnson, O.; Hercules, D. M. *J. Am. Chem. Soc.* **1980**, *102*, 1910.
(48) Joyner, D. J.; Johnson, O.; Hercules, D. M. *J. Phys. F: Met. Phys.* **1980**, *10*, 169.
(49) Joyner, D. J.; Johnson, O.; Hercules, D. M.; Bullett, D. W.; Weaver, J. H. *Phys. Rev. B* **1981**, *24*, 3122.
(50) Joyner, D. J.; Willis, R. F. *Philos. Mag., A* **1981**, *43*, 815.

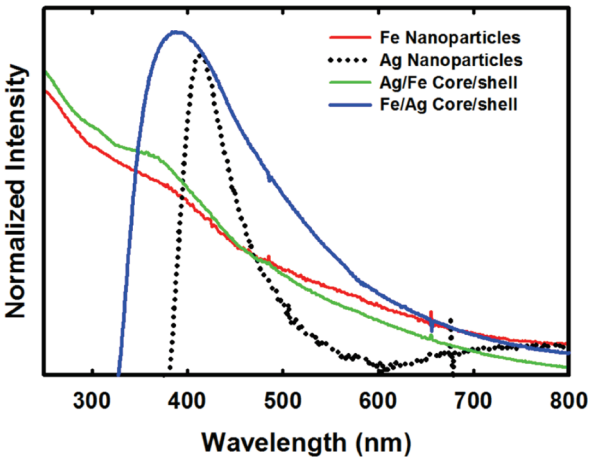

Figure 5. UV−vis absorption spectra of the Fe/Ag (solid blue line), Ag/Fe (solid green line), pure Ag (dotted black line), and pure Fe (solid red line) nanoparticles.

In addition, an increase in the intensity of the ~707 eV peak is seen at various $AgNO_3$ introduction times. This increase is due to the different core/shell formations. Figure 4b is a representative atomic percentage of the core level Ag3d and the Fe2p regions associated with either elemental Fe or FeB/Fe_2B as a function of different introduction times of $AgNO_3$. The atomic percentage was derived from integrated peak areas using standard sensitivity factors and is corrected for the differences in the photoelectron escape depth for both Ag3d and Fe2p. What this suggests is that the surface composition of Fe2p is changing because of the formation and growth of Ag nanoparticles on the surface. These results, along with the other characterization techniques, suggest the formation of Fe/Ag core/shell nanoparticles.

Figure 5 shows UV−vis absorption data of the synthesized Fe/Ag, Ag/Fe, Fe nanoparticles, and Ag nanoparticles showing various plasmon absorption properties. The absorption band of the pure Ag nanoparticles synthesized by the citrate/borohydride method is centered at 410 nm, and is consistent with the literature values.[51−54] A plasmon shift in the absorption band to 380 nm is seen along with a broadening of the band for Fe/Ag core/shell nanoparticles and is due to the small surface layer of Ag.[55] Similar absorption properties are seen when comparing

Scheme 1. Proposed Reaction Scheme for the Reduction of Sodium Citrate, $FeCl_2 \cdot 7H_2O$ and $NaBH_4$; Addition of $AgNO_3$ at Various Times after the Addition of $NaBH_4$ Produced Various Core/Shell Morphologies

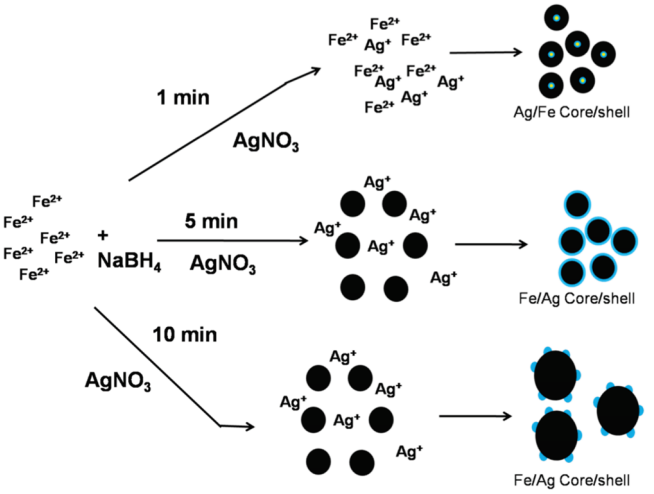

the synthesized pure Fe nanoparticles with the Ag/Fe nanoparticles, consistent with the formation of a Ag core. In addition, the absorption spectra of the synthesized pure Fe nanoparticles are similar to literature data and consists of two small bands at 200 and 360 nm.[56] The band at 200 nm corresponds to the citrate ion while the band at 360 nm corresponds to the small Fe nanoparticles.[57]

4. General Discussion

The above results suggest that the formation of different core/shell structures are determined by the various introduction times of $AgNO_3$ to the reaction vessel after the $NaBH_4$ addition. Scheme 1 depicts how the introduction of $AgNO_3$ at different times after the addition of $NaBH_4$ creates various core/shell structures.

These results can be explained by the differences in the reduction potentials for Fe^{2+} and Ag^+ in an aqueous solution ($E^\circ_{Fe^{2+}/Fe^0} = -0.41$ V vs SHE; $E^\circ_{Ag^{2+}/Ag^0} = +0.80$ V vs SHE).[58,59] In this sense, for the 1 min introduction time after $NaBH_4$ addition, the Ag is formed by classical homogeneous nucleation and growth resulting in 4−5 nm spherical nanoparticles. These Ag nanoparticles serve as nucleation sites for the Fe nanoparticles to grow, which simulates a heterogeneous nucleation and growth process.[52,53,57,60−62] For the 5 min reaction, the Fe nanoparticles have already formed and therefore act as nucleation sites for the Ag nanoparticles to form and grow, creating an Fe/Ag core/shell nanoparticles. Lastly, the 10 min introduction of $AgNO_3$ produces ~150 nm Fe clusters, as previously reported.[34] These Fe clusters again act as nucleation sites for the Ag to form. This scenario creates islands of Ag nanoparticles on the larger Fe clusters.

Although we were unable to definitively determine if the Fe nanoparticles formed were that of elemental Fe, FeB, or Fe_2B, the room temperature VSM data shows that the particles do in fact have a high magnetization saturation (M_s) over 150 emu/g for the 10 min addition of Ag (see Figure S5 in the Supporting Information). This is a higher value than any previously reported FeO_x/Ag or iron boride nanoparticles. For the purpose of this study a saturation magnetization (M_s) was determined by plotting a magnetization versus 1/H and extrapolating to the point where 1/H is equal to zero. The samples prepared with silver nitrate injection times of one minute and five minutes after $NaBH_4$ addition show a saturation magnetization of 105 and 126emu/g, respectively. The changes in the magnetization can be explained by the formation of various core/shell morphologies.

5. Conclusion

We reported on a one-pot aqueous synthesis of Fe/Ag and Ag/Fe core/shell nanoparticles synthesized using sodium borohydride and sodium citrate under ambient conditions. Fe/Ag core/shell nanoparticles with optical and magnetic functionality offer broad opportunities in medicine, catalysis and chemical detection. On the basis of TEM, XAS, and XPS characterization, we demonstrated that varying the addition times of silver nitrate we were able to form various core/shell morphologies consisting of Fe and Ag. For example, if silver nitrate is injected 1 min after sodium borohydride is added to the reaction vessel, Ag will nucleate first followed by Fe, creating monodisperse Ag/Fe core/shell nanoparticles. In contrast, if the introduction time is prolonged to 5 min, Fe nanoparticles will nucleate followed by Ag producing Fe/Ag nanoparticles. This work demonstrates a facile route to chemically manipulating the formation of core/shell nanoparticles and can be tailored to other core/shell systems with relative ease.

Acknowledgment. The authors acknowledge the use of the Centralized Research Facilities in Drexel University's College of Engineering and the MRCAT at the Advanced Photon Source, which are supported by the United States Department of Energy, Office of Science, Basic Energy Sciences Division, and the MRCAT member institutions. This research was also supported in part by the VCU Nanomaterials Core Characterization Facility, School of Engineering Foundation, and a Grant from NSF CHE-0820945 MRI (XPS).

Supporting Information Available: Experimental procedures and additional figures (PDF). This material is available free of charge via the Internet at http://pubs.acs.org.

(51) Medina-Ramirez, I.; Bashir, S.; Luo, Z. P.; Liu, J. L. *Colloids Surf., B* **2009**, *73*, 185.
(52) Prema, P.; Raju, R. *Biotechnol. Bioprocess Eng.* **2009**, *14*, 842.
(53) Ratyakshi; Chauhan, R. P. *Asian J. Chem.* **2009**, *21*, 113.
(54) Sato-Berru, R.; Redon, R.; Vaquez-Olmos, A.; Saniger, J. M. *J. Raman Spectrosc.* **2009**, *40*, 376.
(55) Alvarez-Puebla, R. A.; Aroca, R. F. *Anal. Chem.* **2009**, *81*, 2280.
(56) Blanco, M. C.; Meira, A.; Baldomir, D.; Rivas, J.; Lopezquintela, M. A. *IEEE Trans. Magn.* **1994**, *30*, 739.
(57) Dong, X. Y.; Ji, X. H.; Wu, H. L.; Zhao, L. L.; Li, J.; Yang, W. S. *J. Phys. Chem. C* **2009**, *113*, 6573.
(58) Wiley, B.; Sun, Y.; Xia, Y. *Acc. Chem. Res.* **2007**, *40*, 1067.
(59) Machulek Junior, A.; de Oliveira, H. P.; Gehlen, M. H. *Photochem. Photobiol. Sci.* **2003**, *2*, 921.
(60) Van Hyning, D. L.; Zukoski, C. F. *Langmuir* **1998**, *14*, 7034.
(61) Calvin, S.; Carpenter, E. E.; Harris, V. G. *Phys. Rev. B: Condens. Matter Mater. Phys.* **2003**, *68*, 033411/1.
(62) Carpenter, E. E.; Calvin, S.; Stroud, R. M.; Harris, V. G. *Chem. Mater.* **2003**, *15*, 3245.